Journal of Solid State Chemistry **157,** 339–346 (2001)
doi:10.1006/jssc.2000.9078, available online at http://www.idealibrary.com on IDEAL®

Chemical Reaction of TiAl Intermetallics with a Nitrogen Plasma

Masahiro Inoue, Masanobu Nunogaki, and Katsuaki Suganuma

Institute of Scientific and Industrial Research, Osaka University, 8-1 Mihogaoka, Ibaraki, Osaka 567-0047, Japan

Received September 7, 2000; in revised form December 4, 2000; accepted December 8, 2000; published online February 19, 2001

Direct surface nitridation of TiAl alloy was successfully performed using a reactive plasma process. The modified layer, composed of a double-layer structure, was fabricated using this plasma process. The top surface layer mainly consisted of a ternary nitride, Ti_2AlN. The reaction mechanism in this plasma process is divided into three stages: surface reaction, diffusion of atomic nitrogen, and rearrangement of atomic configuration. The driving force to form the ternary nitride from TiAl was considered by a quantum chemical simulation. As a result of the simulation, the strong Coulomb attractive interaction between Ti and interstitial N atoms in the TiAl alloy is inferred to be predominate in the rearrangement of the atomic configuration, rather than the covalency between Al and N atoms. The surface modified layer significantly exhibits a higher hardness than the TiAl alloy. The subsurface layer retains sufficient ductility, although solution hardening was slightly achieved. © 2001 Academic Press

Key Words: **intermetallics; reactive plasma process; surface treatment; hardness; reaction mechanism; molecular orbital simulation.**

1. INTRODUCTION

TiAl alloys are promising as one of the candidates for novel structural materials in many industries such as the aerospace and automobile industries (1). The microstructural control (1) and the composite material designs (2) have been studied to improve their mechanical properties. In addition to these material designs, surface treatment is an important technique for extending material lifetime because it is expected to improve wear, heat, corrosion, and oxidation resistance. Physical and chemical vapor deposition processes for forming coatings with high melting points, hardnesses, and environmental resistance are being actively studied. However, exfoliation of the coatings, which is caused by large thermal expansion mismatches between the coatings and substrates, is a serious problem in achieving reliable barrier coatings.

One of the present authors (Nunogaki) has developed a novel plasma process (reactive plasma process) for directly transforming metal surfaces to ceramics with the properties of a functionally graded material (3, 4). The reactive plasma process has the following superior points to a conventional ion nitriding process: the sample can be heated to above 1000°C independently of the plasma power, a powerful microwave plasma can be used for scaling of the reactive plasma, and a homogeneous modified layer is obtainable. This paper investigates the nitriding of Ti–48 at. % Al alloys by reactive plasma processing to develop an effective surface treatment of intermetallics and their related materials.

2. EXPERIMENTAL PROCEDURE

2.1. Fabrication and Evaluation

The Ti–48 at. % Al alloy was fabricated by vacuum hot-pressing an alloying powder prepared by self-propagating high-temperature synthesis and mechanical crushing (Kyouritu Ceramic Materials Co., Ltd.). Plates ($5 \times 8 \times 1\,mm^3$) of the alloy were obtained from the hot-pressed disks.

The apparatus and processing details of the reactive plasma process have been described previously (3, 4). In this work, nitridation of the alloy was performed at 1100°C for 2 h. The source plasma was generated using a Penning Ion Gauge (PIG) discharge under a gas pressure of 6.0×10^{-2} Pa ($N_2 : H_2 = 5 : 2$). The cross-sectional microstructure of the modified layers was observed by scanning electron microscopy (SEM). The polished surface was chemically etched with Kroll's reagent for SEM observation. The constitutional phases were identified by X-ray diffraction (XRD). The hardness of the modified layers was characterized by an indentation system (Microzone test system: MZT-4, Akashi Co., Ltd.) with a triangular pyramidal indenter (tip angle: 68°). For the indentation test, a load of up to 98 mN was applied with a loading rate of $49\,mN\,s^{-1}$. After maintaining the maximum load for 5 s, the load was removed at $49\,mN\,s^{-1}$. The hardness was estimated by the equation

$$H = F/A = K \cdot F/h^2, \qquad [1]$$

E-mail: inoue@sanken.osaka-u.ac.jp.

0022-4596/01 $35.00

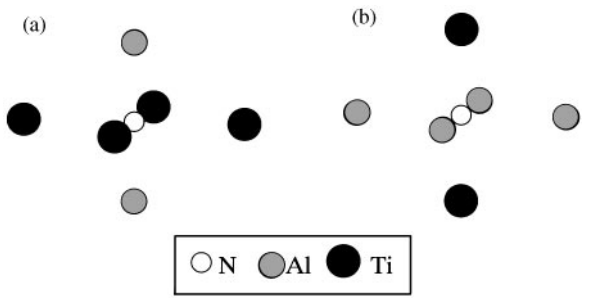

FIG. 1. Cluster models of (a) $Ti_4Al_2N_1$ and (b) $Ti_2Al_4N_1$ before geometrical optimization by an eigenvector-following method.

where H, F, A, K, h are hardness, maximum indentation load (mN), projected area of the hardness impression, geometrical constant (2.972 for the present indenter), and maximum penetration depth (μm), respectively.

2.2. Molecular Orbital Simulation

In order to qualitatively consider the formation mechanism of the modified layers, the molecular orbitals around the interstitial N atoms in the ground state were simulated using several first-principle algorithms. To estimate the lattice distortion by an interstitial N atom, the geometrical optimization of the eigenvector-following method for the cluster models ($Ti_4Al_2N_1$ and $Ti_2Al_4N_1$) illustrated in Figs. 1a and 1b, which represent interstitial atomic nitrogen (N) in the Ti and Al planes of the TiAl alloy, was conducted using a commercial program, namely the Dmol[3] code, with a nonlocal density function of the generalized gradient approximation (GGA) (packaged in Cerius2, Molecular Simulation Inc.). In addition to the geometrical optimization, the total energy of these cluster models was calculated with the Dmol[3] code. By using the result of the geometrical optimization, the cluster models of $Ti_{20}Al_{18}N_1$ and $Ti_{18}Al_{20}N_1$ (Figs. 2a and 2b), which include the distortions by interstitial N atoms, were constructed for the DV-Xα simulation by a program, namely the SCAT code (5–7). Because the convergence to a self-consistent field was barely achieved for these large metallic cluster models by the Dmol[3] code, the DV-Xα method was adopted for the simulation of these models. The Mulliken population analysis was also performed by the SCAT code to obtain useful parameters to qualitatively discuss the bond nature, such as bond overlap

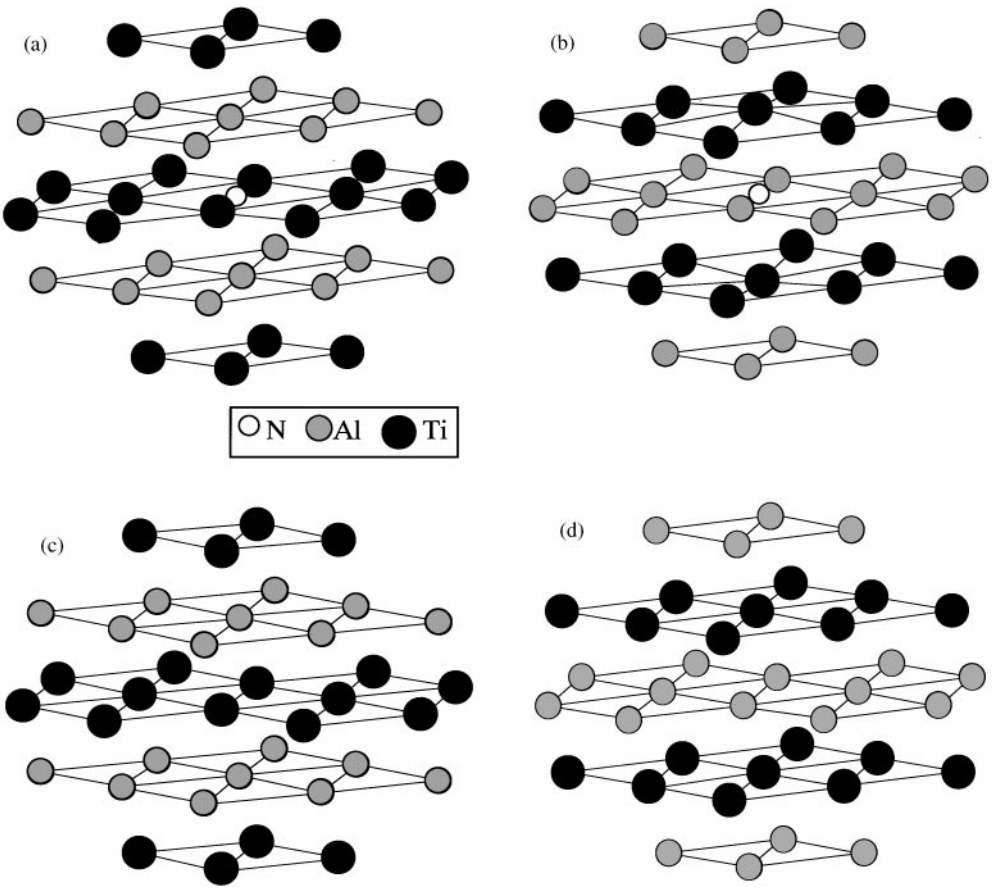

FIG. 2. Cluster models of (a) $Ti_{20}Al_{18}N_1$ and (b) $Ti_{18}Al_{20}N_1$ including the lattice distortion of nearest-neighbor Ti and Al atoms induced by N atoms. Cluster models (c) $Ti_{20}Al_{18}$ and (d) $Ti_{18}Al_{20}$ are reference clusters for models (a) and (b), respectively.

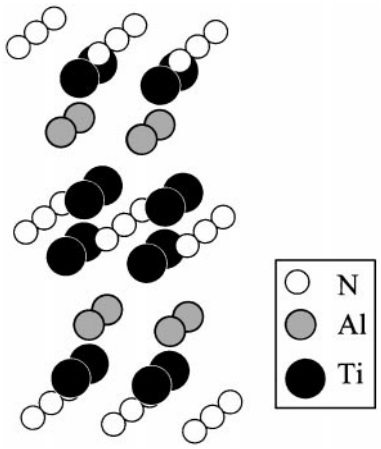

FIG. 3. Cluster model of $Ti_{16}Al_8N_{27}$, which is extracted from the crystal structure of Ti_2AlN.

population and net change. Furthermore, DV-Xα simulation of the cluster model of the $Ti_{16}Al_8N_{27}$ shown in Fig. 3, which is extracted from the Ti_2AlN crystal, was conducted to understand the characteristics of chemical bonds in this ternary nitride. Madelung potentials were not arranged around the cluster models for the first-principle simulations. The energy levels of the molecular orbitals are shifted to set the highest occupied orbital at 0.

3. RESULTS AND DISCUSSION

3.1. Microstructure of Modified Layer

Figure 4 shows the typical cross-sectional microstructure of the surface of the Ti–48 at. % Al substrate nitrided by a reactive plasma process at 1100°C for 2 h. The surface

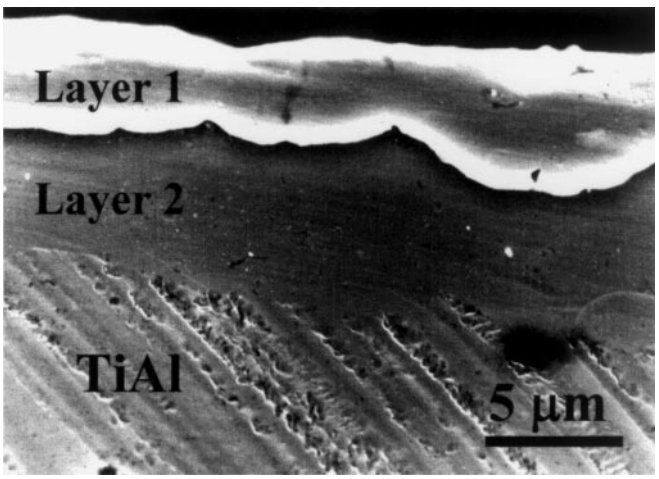

FIG. 4. Cross-sectional SEM micrograph of the surface modified layer fabricated by the reactive plasma process at 1100°C for 2 h.

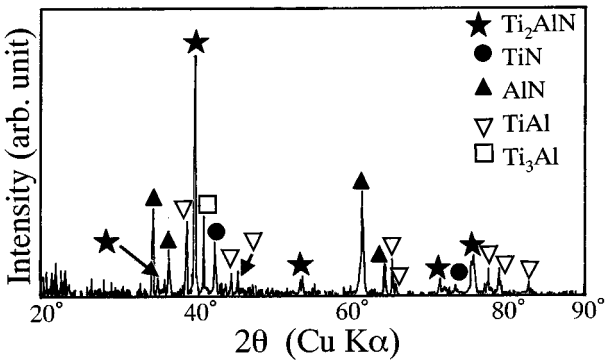

FIG. 5. XRD pattern of the specimen after reactive plasma processing.

modified layers consist of two layers that are formed on the TiAl alloy with a lamella structure. The alloy was composed of the lamella structure TiAl and Ti_3Al phases before the surface treatment. The XRD pattern in Fig. 5, measured using X-rays incident perpendicular to the sample surface, indicates that the main phase of the modified layer is Ti_2AlN. Signs of AlN and TiN formation as byproducts are also observed in this figure. The subsurface layer (layer 2) is considered to be a diffusion layer of interstitial N atoms.

3.2. Formation Mechanism of Ti_2AlN Layer

The formation process of the modified layers is briefly divided into three steps, i.e., (1) surface reaction, (2) diffusion of atomic nitrogen (N), and (3) rearrangement of the atomic configuration (formation of reaction product). In this plasma-processing apparatus, the gas mixture of N_2 and H_2 was transformed to a reactive plasma using a PIG-type discharge, which is a type of radio frequency (RF) discharge utilizing a tandem motion of electrons with acceleration and deceleration between a hot tungsten filament and an anticathode at low gas pressure. This reactive plasma contained abundant ions and molecules (N^+, NH_3, etc.) in excited states. The effective excitation of chemical species in the plasma results in decreasing the activation energy for diffusing N into the alloy. When the chemical potential of the N reaches a critical value in the alloy, the rearrangement of atomic configuration should occur to form Ti_2AlN.

In order to consider the formation mechanism of the Ti_2AlN, the chemical environments around the interstitial N in the TiAl were simulated by the quantum chemical algorithms. TiAl has an $L1_0$-type crystal structure that contains alternately stacked Ti and Al planes in the direction of the *c* axis (1). In the present simulation, the interstitial N atoms are arranged in these planes. As a result of geometrical optimization for the cluster models of the $Ti_4Al_2N_1$ and $Ti_2Al_4N_1$ (Figs. 1a and b) by an eigenvector-following method, an anisotropic distortion of the lattice is

predicted to be induced by the interstitial N atoms. Due to the interstitial N atoms in the Ti plane, the nearest-neighbor Ti and Al atoms are forced to be 11.60 and 0.61% further from the standard positions in TiAl, respectively (Table 1a). However, the interstitial N atoms in the Al plane forces nearest-neighbor Al and Ti atoms to be 5.38 and 8.17% further from the standard positions in TiAl, respectively (Table 1b).

To briefly estimate the relative energetic difference between these atomic configurations, the following reactions are assumed

$$4\mathrm{Ti} + 4\mathrm{Al} + \mathrm{N} \rightarrow \mathrm{Ti_4Al_2N_1} + 2\mathrm{Al}, \quad [2]$$

$$4\mathrm{Ti} + 4\mathrm{Al} + \mathrm{N} \rightarrow \mathrm{Ti_2Al_4N_1} + 2\mathrm{Ti}, \quad [3]$$

where Al, Ti, and N are the isolated atoms. Thus, the energetic stability of these clusters can be compared by the formula

$$\mathrm{Ti_4Al_2N_1} + 2\mathrm{Al} \rightarrow \mathrm{Ti_2Al_4N_1} + 2\mathrm{Ti}. \quad [4]$$

The total energies of $Ti_4Al_2N_1$, $Ti_2Al_4N_1$, Al, Ti are shown in Table 2. The energetic difference in the reaction [4] is estimated:

$$\Delta E_{\mathrm{total}} = \{E(\mathrm{Ti_2Al_4N_1}) + 2E(\mathrm{Ti})\} - \{E(\mathrm{Ti_4Al_2N_1}) + 2E(\mathrm{Al})\} = 1.24\ \mathrm{eV}. \quad [5]$$

Therefore, the atomic configuration in the $Ti_4Al_2N_1$ cluster is more stable than that in the $Ti_2Al_4N_1$ cluster. Although the precise estimation of defect energies, which is based on the total energy of crystal using a model with a periodic boundary condition, is necessary to discuss the stability of defect structures, the stable atomic configuration for the interstitial N atoms is briefly inferred by the above consideration. The interstitial N atoms in the Ti planes are expected to be more stable than those in the Al planes.

TABLE 1
Results of the Geometrical Optimization of the $Ti_4Al_2N_1$ and $Ti_2Al_4N_1$ Clusters

Bond	Interatomic distance (nm)
(a) Cluster model: $Ti_4Al_2N_1$	
Initial	
N–Ti	0.19995
N–Al	0.20400
Optimized	
N–Ti	0.22214
N–Al	0.20525
(b) Cluster model: $Ti_2Al_4N_1$	
Initial	
N–Al	0.19995
N–Ti	0.20400
Optimized	
N–Al	0.21070
N–Ti	0.22067

TABLE 2
Total Energy of the Clusters and Atoms Calculated by the Dmol^3 Code

Models	Ti_4Al_2N	Ti_2Al_4N	Al	Ti
Total energy ($\times 10^3$ eV)	− 107.71783	− 74.13131	− 6.59841	− 23.12130

Based on these calculation results, the cluster models of $Ti_{20}Al_{18}N_1$ and $Ti_{18}Al_{20}N_1$, which include the geometrically optimized clusters of $Ti_4Al_2N_1$ and $Ti_2Al_4N_1$ as a central unit, are constructed as shown in Figs. 2a and 2b. To obtain qualitative information about the chemical bonds, the DV-Xα simulation of these models was conducted with and without interstitial N atoms in $Ti_{20}Al_{18}$ and $Ti_{18}Al_{20}$ (Figs. 2a–d).

Figures 6a and 6b show the bond overlap population and net charge in the cluster models of $Ti_{20}Al_{18}$ and $Ti_{20}Al_{18}N_1$ respectively, which represent the interstitial N atoms in the Ti plane. The net charge values indicate significant charge transfer to N atoms from neighbor Ti and Al atoms. In addition to the charge transfer, the covalent bond strength of the Al–Ti and Ti–Ti bonds, which is in proportion to the bond overlap population, decreases with interspersing N atoms. Figure 7b shows the overlap population diagram for the chemical bonds of an N atom with first nearest-neighbor Ti and Al atoms for the $Ti_{20}Al_{18}N_1$ cluster model. By comparison with the results of the partial density of state illustrated in Fig. 7a, the atomic orbital components that contribute to forming these chemical bonds can be deduced. The Ti–N bonds have a relatively low-bond overlap population due to the lack of bonding components from Ti 3*d* orbitals, although the N 2*p* components significantly contribute with bonding characteristics. However, the net charge of the N and Ti atoms indicates that the stability of the Ti–N bonds in the Ti planes is compensated by the strong ionic attractive interaction between these atoms. In contrast, the chemical bonds of the N atom with neighbor Al atoms exhibit significant covalency that originates from hybridization of the *sp* components.

Figures 8a and 8b show the bond overlap population and net charge in the clusters of $Ti_{18}Al_{20}$ and $Ti_{18}Al_{20}N_1$, which represents the interstitial N atoms in the Al plane. In this

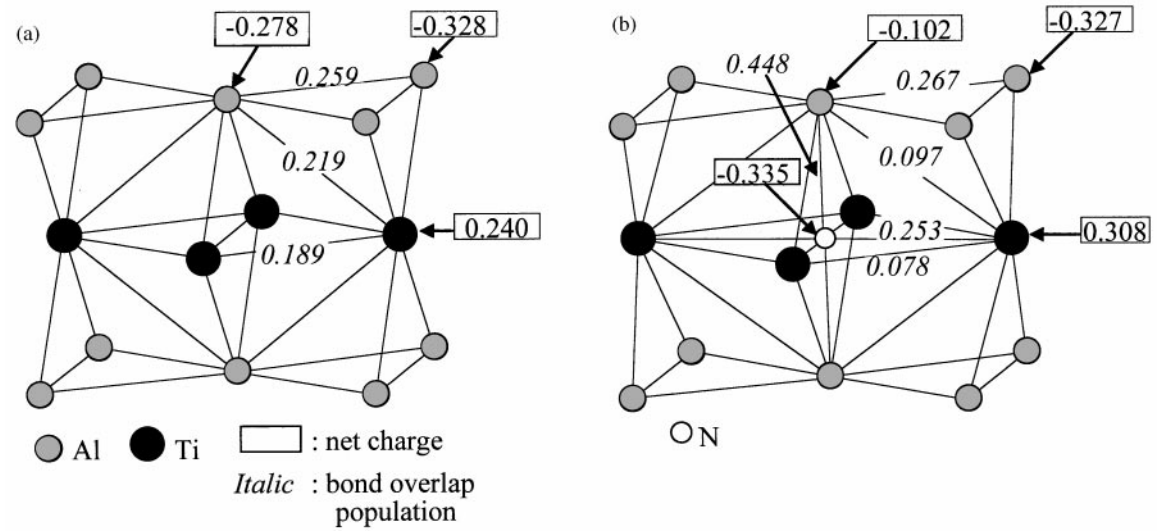

FIG. 6. Bond overlap population and net charge in central units of the (a) $Ti_{20}Al_{18}$ and (b) $Ti_{20}Al_{18}N_1$ cluster models. A central unit of the cluster model is only indicated in this figure.

situation, the charge transfer to an N atom mostly occurs from neighboring Al atoms. Moreover, the covalent bond strength of the Al–Al and Al–Ti bonds is reduced by the N atom. Figure 9b shows the overlap population diagram for the chemical bonds of the N atom with first nearest-neighbor Al and Ti atoms of the $Ti_{18}Al_{20}N_1$ cluster model. Although the characteristics of chemical bonds in this model are analogous to that in the $Ti_{20}Al_{18}N_1$ cluster model, two different features are clarified by the results of this calculation. The first is insufficient ionic attraction for compensation for the low-bond overlap population between the N and Ti atoms. Another feature is the anti-bonding interactions that create energy levels with anti-bonding characteristics on the highest occupied level. In this atomic configuration, the contribution of anti-bonding components is much larger than that in the $Ti_{20}Al_{18}N_1$ model. The anti-bonding components are also considered to be one of the factors for energetic destabilization.

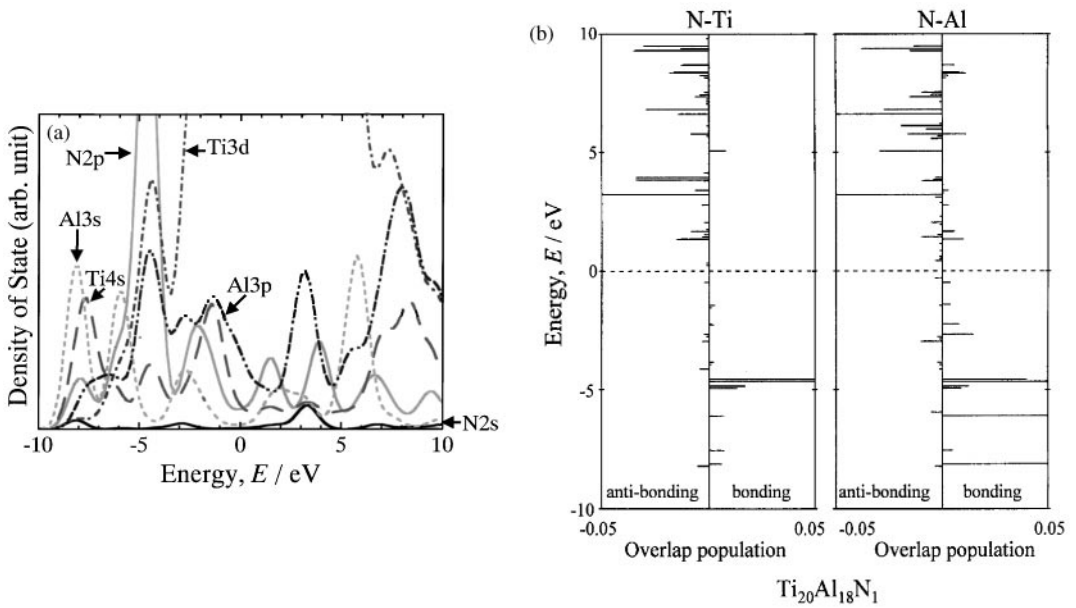

FIG. 7. (a) Partial density of state in the $Ti_{20}Al_{18}N_1$ cluster model. (b) Overlap population diagram for the N–Ti and N–Al bonds.

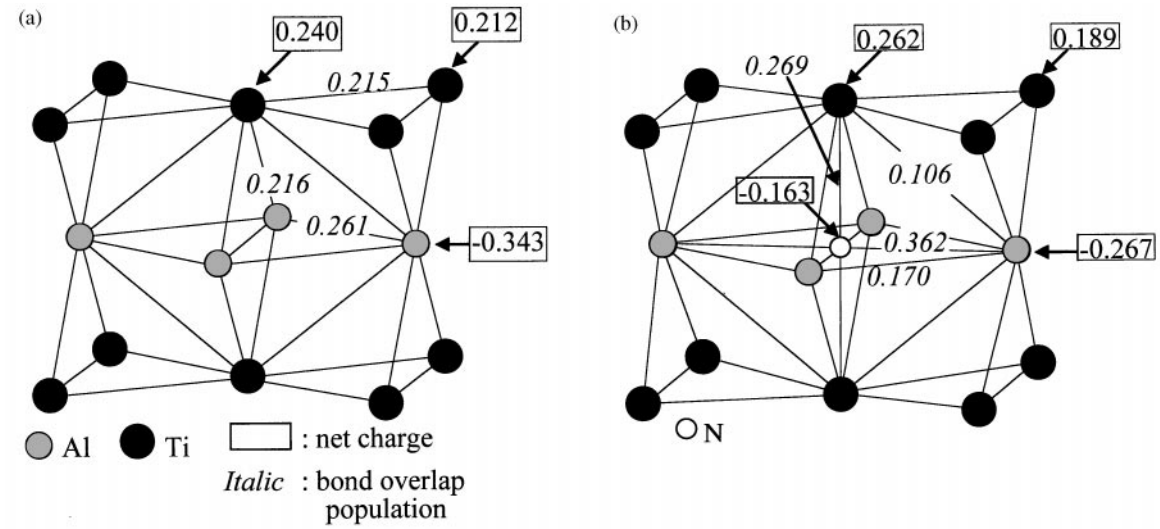

FIG. 8. Bond overlap population and net charge in central units of the (a) $Ti_{18}Al_{20}$ and (b) $Ti_{18}Al_{20}N_1$ cluster models. A central unit of the cluster model is only indicated in this figure.

Although the rearrangement process of atomic configuration to form Ti_2AlN cannot be wholly explained by local atomic interactions, it is likely to be based on these characteristic chemical interactions between the interstitial N and neighboring atoms. Figure 10 shows the results of the DV-Xα simulation for the $Ti_{16}Al_8N_{27}$ cluster model that is constructed from the crystal structure of Ti_2AlN. To simply understand the characteristics of the chemical bonds, Fig. 10 only shows the results of a central unit in the cluster model. The result of population analysis for the $Ti_{16}Al_8N_{27}$ cluster model shows that the covalent bonds are not formed between neighboring N atoms. The Coulomb repulsive interaction is also induced between these N atoms. Hence, the atomic configuration of the N atoms is determined by competition between the ionicity of the Ti–N bonds and the covalency of the Al–N bonds in the TiAl alloy, but not clustering of N atoms.

The net charge of neighboring Ti and N atoms in the $Ti_{16}Al_8N_{27}$ cluster indicates significant charge transfer from Ti atoms to N atoms. Strong covalent bonds, as well as the

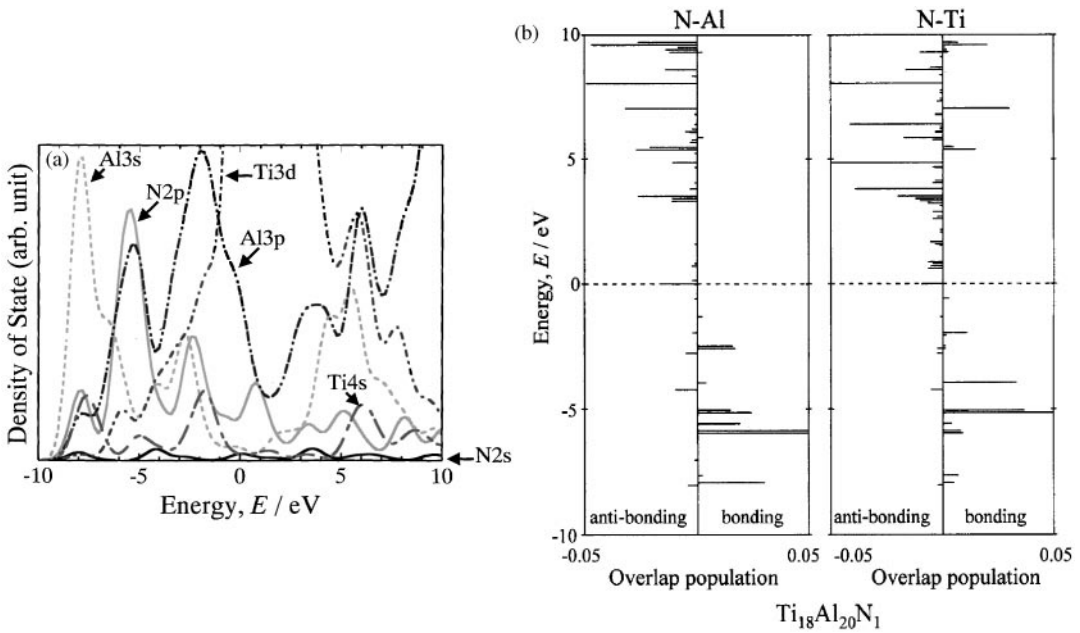

FIG. 9. (a) Partial density of state in the $Ti_{18}Al_{20}N_1$ cluster model. (b) Overlap population diagram for the N–Ti and N–Al bonds.

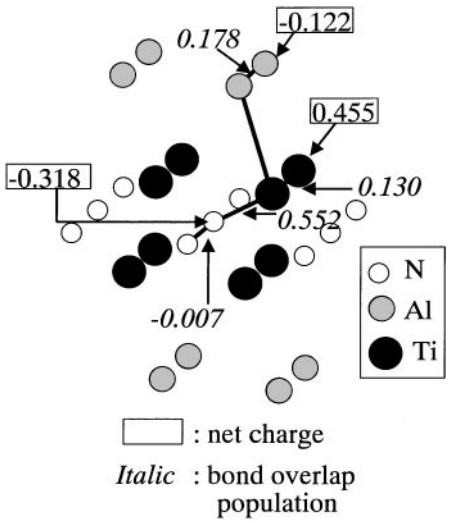

FIG. 10. Results of molecular orbital simulation for the $Ti_{16}Al_8N_{27}$ cluster. A central unit of the cluster model is only indicated in this figure.

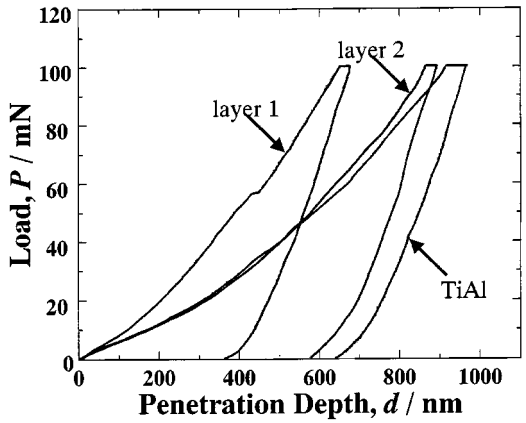

FIG. 11. Loading–unloading profiles of the Ti–48 at. % Al substrate, layers 1 and 2, during the indentation test with a triangular pyramidal indenter (tip angle: 68°).

Coloumb attractive force, can be formed between the Ti and N atoms because of the high-bond overlap population. Therefore, the strong Coulomb attractive interaction between the Ti and N atoms is inferred to play an important role in rearranging the atomic configuration from TiAl to Ti_2AlN, rather than the strong covalency between Al and N atoms. The stability of the $Ti_4Al_2N_1$ cluster suggests that the interstitial N atoms in the Ti planes of TiAl contribute to the rearrangement of the atomic configuration, rather than those in the Al plane. Thus, the interstitial N atoms in the Ti planes are expected to make a predominant contribution for forming a Ti_2AlN lattice. After the rearrangement of the atomic configuration, the strong covalency, as well as the ionic attractive interaction, is created between Ti and N atoms.

3.3. Mechanical Behavior of Modified Layer

Figure 11 and Table 3 show loading–unloading profiles and deformation properties of the Ti–48 at. % Al substrate, with layers 1 and 2 being measured by the indentation test with a triangular pyramidal indenter. Layer 1, which is mainly composed of Ti_2AlN, has a hardness two times higher than that of the TiAl substrate. Because Ti_2AlN has a complicated crystal structure with alternate stacking of polarized layers as shown in Fig. 7 (8, 9), the dislocation motion is extremely suppressed, resulting in a high hardness. The modified layer with a high hardness is expected to improve its wear resistance. Although the modified layer has a superior hardness, it is intrinsically brittle due to low plastic deformability. Hence, toughness of the interface between the modified layer and the matrix alloy is an important factor in determining the exfoliation resistance of the layer. In the subsurface (layer 2), solution hardening by the interstitial N atoms is slightly observed as shown in Fig. 9. The N atoms can provide significant hardening by two main mechanisms: local distortion of the lattice and modulation of the Coulomb potential by the negatively charged N atoms. However, the layer retains a relatively high plastic deformability, which is expected to achieve a sufficient reliability of interfacial adhesion. The modified layer is considered to have a more reliable adhesion to the TiAl alloy than to coatings formed by physical vapor deposition.

TABLE 3
Deformation Properties of the Ti–48 at. % Al Substrate

	Hardness[a]	Total deformation (nm)	Plastic deformation (nm)	Elastic recovery (%)	Deformation during holding at 98 mN (nm)
Layer 1	641	674	360	46.6	26
Layer 2	359	901	573	36.4	30
TiAl alloy	313	964	638	33.8	50

Note. Layers 1 and 2 are measured by the indentation test illustrated in Fig. 11.
[a]Calculated by Eq. [1].

4. SUMMARY

Direct surface modification of a Ti–48 at. % Al alloy was successfully performed at a substrate temperature of 1100°C using a reactive nitrogen plasma generated at low gas pressure. The modified layer consists of a double-layer structure formed on the substrate. The top surface layer, which has a high hardness, is mainly composed of Ti_2AlN. The rearrangement of the atomic configuration to form Ti_2AlN is predominantly governed by the strong attractive ionicity between the Ti and the interstitial N atoms in the TiAl alloy. The subsurface layer retains a sufficient plastic deformability, although slight solution hardening is induced by local distortion of the lattice and modulation of the Coulomb potential.

ACKNOWLEDGMENTS

The authors thank Mr. J. Tani and Dr. H. Kido, Department of Inorganic Chemistry, Osaka Municipal Technical Research Institute, for cooperation in utilizing the Dmol[3] code of the Cerius2 system for geometry optimization of cluster models.

REFERENCES

1. S. C. Huang and J. C. Chesnutt, *in* "Intermetallic Compounds: Vol. 2" (J. H. Westbrook and R. L. Fleischer, Eds.), Chap. 4, pp. 73–90. J. Wiley, Chichester, UK, 1995.
2. S. M. Jeng, J.-M. Yang, and J. A. Graves, *J. Mater. Res.* **8,** 905–915 (1993).
3. M. Nunogaki, Y. Susuki, K. Kitahama, Y. Nakata, F. Hori, R. Oshima, and S. Emura, *Proc. Mater. Res. Soc. Symp.* **551,** 303–308 (1999).
4. M. Nunogaki, Y. Susuki, and A. Ohmura, *Mater. Design*, in press.
5. H. Adachi, M. Tsukada, and C. Satoko, *J. Phys. Soc. Jpn.* **45,** 875–883 (1978).
6. M. Morinaga, J. Saito, N. Yukawa, and H. Adachi, *Acta Metall. Mater.* **38,** 25–29 (1990).
7. M. Mizuno, I. Tanaka, and H. Adachi, *Phys. Rev. B* **59,** 15,033–15,047 (1999).
8. J. C. Schuster and J. Bauer, *J. Solid State Chem.* **53,** 260–265 (1984).
9. O. Knotek and T. Leyendecker, *J. Solid State Chem.* **70,** 318–322 (1987).